

# EFFECT OF SUBSURFACE DEFECTS ON THE SURFACE TOPOGRAPHY OF ADDITIVELY MANUFACTURED COMPONENTS

Zachary C. Reese<sup>1</sup>, Jason Fox<sup>2</sup>, Felix Kim<sup>2</sup>, John Taylor<sup>1</sup>, and Chris Evans<sup>1</sup>

<sup>1</sup>Center for Precision Metrology

University of North Carolina at Charlotte

Charlotte, North Carolina, USA

<sup>2</sup>The National Institute of Standards and Technology\*

Gaithersburg, Maryland, USA

## ABSTRACT

Additively manufactured (AM) components exhibit an abundance of surface textures and patterns. Past work investigating components created through laser powder bed fusion (LPBF) has shown that these patterns, specifically the chevron resulting from solidification of the melt pool on upward facing surfaces, can be correlated to quality of the final part [1]. Additionally, these patterns as well as the scan tracks have been observed to vary around the region of potential subsurface defects based on flash thermography data. This work explores parts with seeded subsurface defects at various depths from the top surface that are printed in nickel alloy 625 on a commercially available LPBF machine. Surface height maps are obtained using a scanning white light interferometer (SWLI) to determine the defect's impact on the surface texture of subsequent layers. Data obtained from the SWLI are aligned with data from X-ray computed tomography (XCT) to confirm the locations of defects and applicability of this approach as an in-situ detection method is discussed.

## INTRODUCTION

Laser powder bed fusion (LPBF) is an additive manufacturing (AM) process that uses a high-power laser to selectively melt layers of metal powder. These layers are built up from an underlying substrate to form a three-dimensional structure. While the manufacturing method allows for almost unlimited design capacity, the process

itself is not without issues [2]. LPBF parts take on the order of hours or days to build, suffer from poor "as printed" surface texture, and potentially harbor unseen internal defects. This, plus the potential for part-to-part variation, inhibits the qualification and certification of AM parts for aerospace applications [2]. The internal defects, such as porosity and lack of fusion, are only found through destructive or nondestructive secondary analysis of the parts which can be costly and time consuming. Additionally, options for defect analysis become slim if one wants to keep the part intact. Flash thermography has shown some promise; however, it is limited on the depth of the defect that can be observed. X-ray computed tomography (XCT) is a viable option, but requires expertise and expensive equipment for analysis. Currently these analysis methods, both destructive and nondestructive, can only be conducted ex-situ when the part is complete, and it is far too late to remedy the defect. In-situ observation and recognition of deviations during the printing process are required if defects are to be fixed before the part is complete. Currently there is no reliable method of defect recognition during the printing process. However, understanding "as-printed" surface features may be the first step toward an in-situ method for defect detection.

Historically, these complex surfaces were being categorized by their average roughness ( $R_a$ ) values alone; however, it has been shown that

---

\*Official contribution of the National Institute of Standards and Technology (NIST); not subject to copyright in the USA. The full descriptions of the procedures used in this paper require the identification of certain commercial products. The inclusion of such information should in no way be construed as indicating that such products are endorsed by NIST or are recommended by NIST or that they are necessarily the best materials, instruments, software, or suppliers for the purposes described.

these classical parameters prove to be similar for visibly different surfaces [4-6]. This has driven a push away from using classical parameters for surface characterization. Rather, many researchers are beginning to rely on surface features to characterize metal AM parts [3-6]. In previous works, the authors have shown the connection of the chevron pattern on the top of scan lines, seen in Figure 1, to the laser parameters set for the build. A parallel study utilizing flash thermography on parts created through LBPF showed potential subsurface defects. Scanning electron microscope (SEM) images were taken at the site of the potential defect to observe any difference in surface texture. Figure 2 shows that the scan lines lose all definition in the area above the potential defect. The chevron pattern also seems to almost disappear. Upon investigation of the other potential defect sites, a pattern of flattened scan lines with no distinct boundaries emerged. In order to study this phenomenon under controlled conditions, parts with seeded defects were conceived and printed.

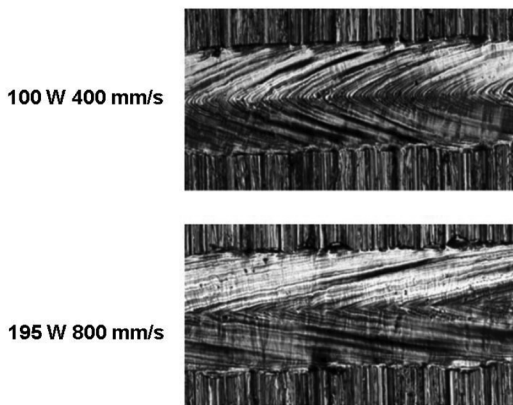


FIGURE 1. Variation in chevron pattern between different laser power and velocity combinations.

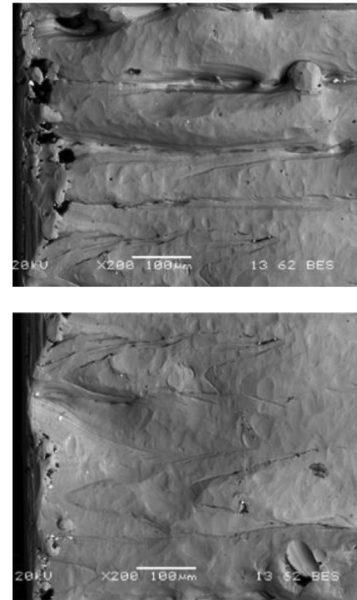


FIGURE 2. SEM image over largest potential defect (bottom). Return of scan lines away from defect (top).

### Methodology

The largest hurdle in designing these parts comes in deterministically planning and creating stochastic defects. Defects are not only created in the surface through user error such as poor parameter selection, but also can occur randomly due to the chaotic nature of the printing process. The goal of the defect artifact is to encapsulate as many of these conditions in which defects can occur as possible. Three defect conditions were settled on: open hole, keyholing, and lack of fusion. Open hole defects are cylindrical areas of powder left purposely un-melted (Figure 3A). Keyhole defects were printed with the recommended laser power and half the recommended laser velocity to ensure the deposition was melting in a keyhole mode (Figure 3B). In the lack of fusion defects, the nominal hatch spacing was doubled to give subsequent printed layers issues in adhering to the defect area (Figure 3C). Defects are printed in a known grid pattern into the square artifact base. All are printed as cylinders ranging from 0.5 mm to 2.5 mm in diameter (Figure 4). The first two columns in Figure 4 (left to right) are left open to air (open air) in order to realize a local coordinate system. The rest are printed over with up to eight subsequent layers to better understand how these defects may propagate throughout a build.

The artifact is built like a staircase in that each column after the open-air defects has one more layer than the previous, and the final column is covered with eight layers (320  $\mu\text{m}$ ) (Figure 5). Four artifacts were printed at defect depths from two to ten layers (80  $\mu\text{m}$  to 400  $\mu\text{m}$ ) deep to understand the size of seeded defect that could reliably be printed. All artifacts were made of nickel alloy 625 in an EOS M290 Direct Metal Laser Sintering (DMLS) machine.

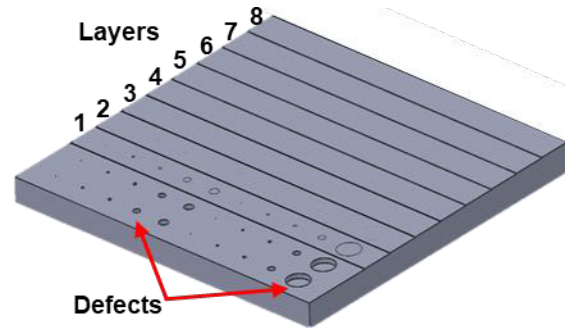


FIGURE 5. Final computer aided design model for defect artifact.

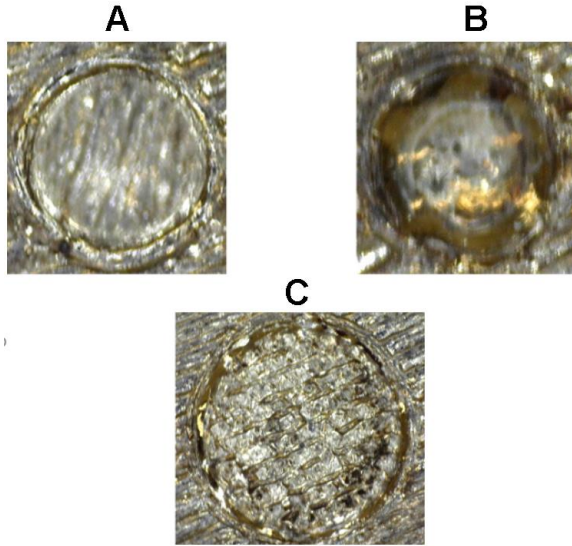


FIGURE 3. Microscope images of open-air defects A) Open hole B) Keyhole C) Lack of fusion.

### Results and Discussion

Once the artifacts were built, they were subject to X-ray computed tomography (XCT) analysis to ensure that the defects that have been printed over still exist within the part. Parts were sent to North Carolina Agricultural and Technical State University (NC A&T) for preliminary XCT analysis. It can be seen in Figure 6 that in the artifact with the deepest seeded defects (ten layers or 400  $\mu\text{m}$ ), all defect types are present within the surface and the largest diameter defects of each type persist throughout the entire build with up to eight layers on top.

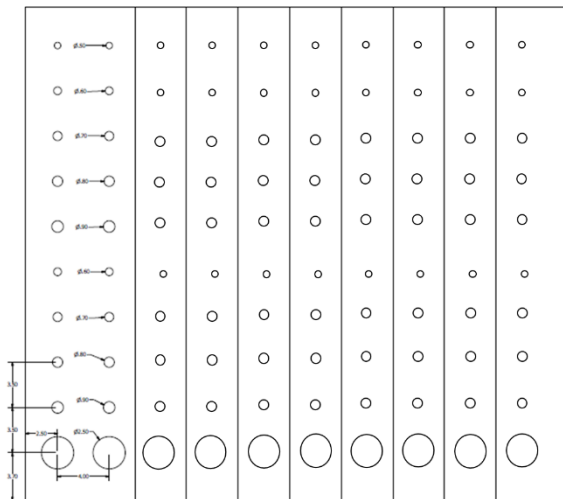


FIGURE 4. Grid pattern and size of defects in the artifact

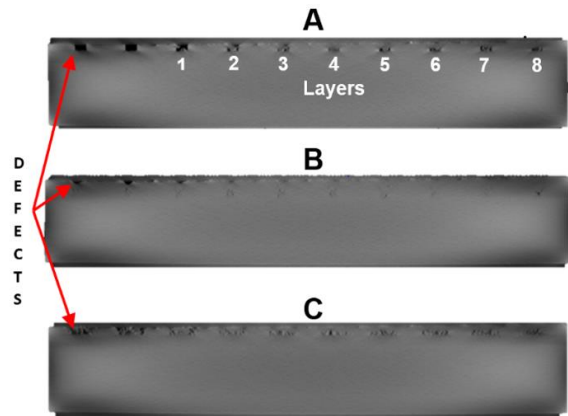


Figure 6. Defects propagating through build (0-8 layers from left to right). A) Open hole B) Keyhole C) Lack of Fusion

Areal surface data was obtained through a commercially available coherence scanning interferometer (CSI) and processed using the packaged software. To capture these defects, up to 100 sites of areal data with a field of view (FOV) of 418  $\mu\text{m}$  x 418  $\mu\text{m}$  were stitched together to encompass the area of the defect and outside

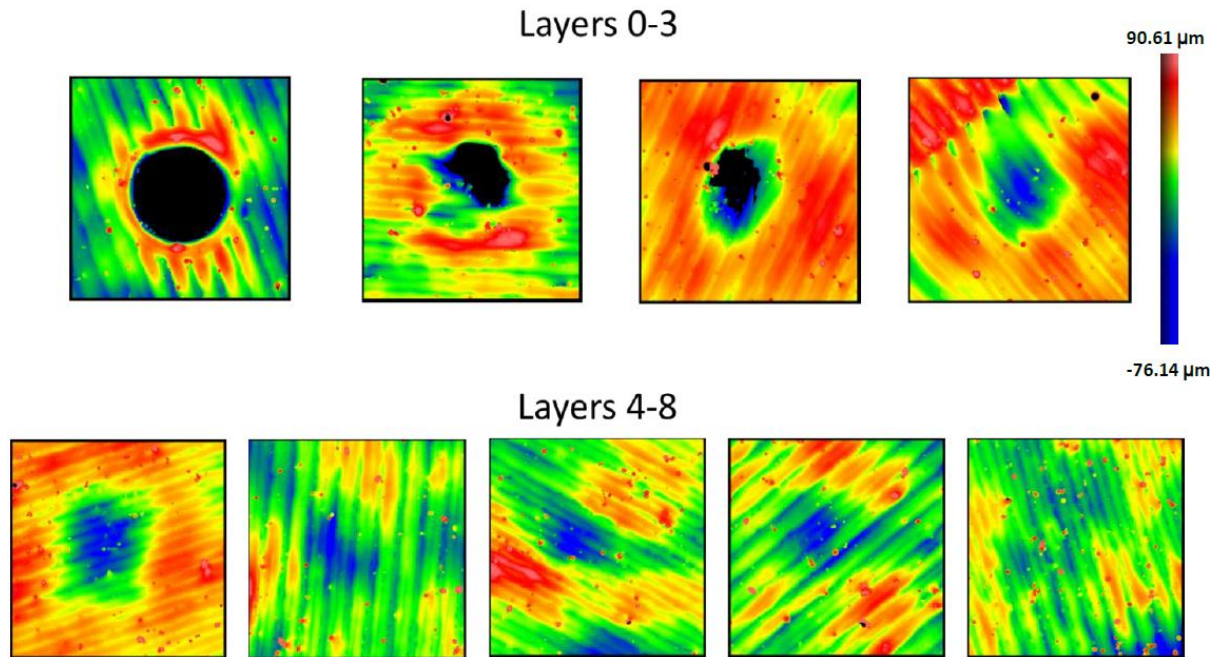


FIGURE 7. Surface topography evolution of open hole defect from 0 to 8 layers (2.25 mm x 2.25 mm FOV)

surrounding topography to view any lateral propagation that may take place as the layers are built on top of the defects. Figure 7 shows the evolution of the surface topography as the largest open hole defect goes from open air up to eight layers deep. One can see that a defect of this size takes a full three layers to fill over the defect itself. Additionally, there is a prominent sag in the spot of the defect throughout the build. At the center of this sag, it is apparent that the scan lines are losing their independence as seen in the SEM data from Figure 2. This correlates with the preliminary surface topography results found in the stochastic defect in the real-world part. The flattened scan lines are just half of the correlation between the defect artifacts and the first part analyzed. Applying a Fourier filter to the area map of the eighth layer reveals that the chevron pattern ceases to exist (Figure 8). It is theorized that the disappearance of the pattern has to do with the altered heat transfer properties of building over and around the seeded defect; however, in-depth microstructural analysis is needed to confirm this.

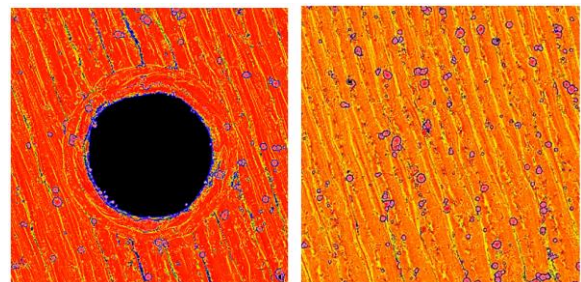


FIGURE 8. Chevron pattern adjacent to seeded defect (left). Lack of chevron pattern on eighth layer above defect

#### FUTURE WORK

While preliminary analysis is promising, a lot of analysis is yet to be done to prove the correlation between subsurface defects and change in the scan lines and chevron pattern seen on the upward facing surfaces. Higher fidelity XCT of defects removed from the artifact via wire electrical discharge machining (EDM) will be used to estimate the size of the initial voids as well as investigate any micro-scale porosity that may propagate throughout the part. Microstructural analysis will be completed to understand how these defects affect the expected microstructure. Finally, another series

of builds is being completed to see if the pattern holds for deeper defects (up to 30 layers).

## ACKNOWLEDGEMENTS

The authors would like to thank the NC A&T team for the XCT analysis of these parts.

## REFERENCES

- [1] Gockel, Joy, and Jack Beuth. "Understanding Ti-6Al-4V microstructure control in additive manufacturing via process maps." *Solid Freeform Fabrication Proceedings, Austin, TX, Aug (2013)*: 12-14.
- [2] Energetics Inc. for National Institute of Standards and Technology. "Measurement science roadmap for metal-based additive manufacturing" (2013). [http://www.nist.gov/el/isd/upload/NISTAdd\\_Mfg\\_Report\\_FINAL-2.pdf](http://www.nist.gov/el/isd/upload/NISTAdd_Mfg_Report_FINAL-2.pdf) (accessed December 15, 2014).
- [3] Z. Reese *et.al.* Observations on the surface morphology of laser powder bed fusion metal surfaces. Met and Props 2017, June 2017, Gothenburg, Sweden. Unpublished conference paper, 2017.
- [4] Fox, Jason C., Shawn P. Moylan, and Brandon M. Lane. "PRELIMINARY STUDY TOWARD SURFACE TEXTURE AS A PROCESS SIGNATURE IN LASER POWDER BED FUSION ADDITIVE MANUFACTURING." *2016 Summer Topical Meeting: Dimensional Accuracy and Surface Finish in Additive Manufacturing*. 2016.
- [5] Fox JC, Moylan SP, Lane BM. Effect of process parameters on the surface roughness of overhanging structures in laser powder bed fusion additive manufacturing. *Procedia CIRP*, Charlotte, NC: 2016. doi:10.1016/j.procir.2016.02.347
- [6] Senin, Nicola, and Richard K. Leach. "Information-rich surface metrology." *Procedia CIRP* (2018).